



OPEN ACCESS

EDITED BY

Longlu Wang,
Nanjing University of Posts and
Telecommunications, China

REVIEWED BY

Liu Xia,
Qingdao University, China
Weiwei Zhao,
Nanjing University of Posts and
Telecommunications, China

*CORRESPONDENCE

Hong-Zhang Geng,
genghz@tiangong.edu.cn
Lianzhong Zhang,
zlj8777@163.com

[†]These authors have contributed equally
to this work.

SPECIALTY SECTION

This article was submitted to
Nanoscience,
a section of the journal
Frontiers in Chemistry

RECEIVED 19 June 2022

ACCEPTED 07 July 2022

PUBLISHED 05 August 2022

CITATION

Wang Y, Wang T, Liu Y, Geng H-Z and
Zhang L (2022), Environment-friendly
AgNWs/Ti₃C₂T_x transparent conductive
film based on natural fish gelatin for
degradable electronics.
Front. Chem. 10:973115.
doi: 10.3389/fchem.2022.973115

COPYRIGHT

© 2022 Wang, Wang, Liu, Geng and
Zhang. This is an open-access article
distributed under the terms of the
[Creative Commons Attribution License
\(CC BY\)](https://creativecommons.org/licenses/by/4.0/). The use, distribution or
reproduction in other forums is
permitted, provided the original
author(s) and the copyright owner(s) are
credited and that the original
publication in this journal is cited, in
accordance with accepted academic
practice. No use, distribution or
reproduction is permitted which does
not comply with these terms.

Environment-friendly AgNWs/ Ti₃C₂T_x transparent conductive film based on natural fish gelatin for degradable electronics

Yuzhou Wang^{1,2,3†}, Tao Wang^{3,4†}, Yan Liu², Hong-Zhang Geng^{3*}
and Lianzhong Zhang^{1*}

¹Henan Engineering Technology Research Center of Ultrasonic Molecular Imaging and
Nanotechnology, Henan Provincial People's Hospital, People's Hospital of Zhengzhou University,
Zhengzhou, China, ²College of Materials Engineering, Henan University of Engineering, Zhengzhou,
China, ³Tianjin Key Laboratory of Advanced Fibers and Energy Storage, School of Material Science and
Engineering, Tiangong University, Tianjin, China, ⁴Sinopec Petroleum Engineering Zhongyuan
Corporation, Zhengzhou, China

Recently, the electronic waste (E-waste) has become the most serious environmental trouble because of the iteration of electronic products. Transparent conductive films (TCFs) are the key component of flexible electronic devices, so the development of devices based on degradable TCFs has become an important way to alleviate the problem of E-waste. Gelatin, one of the most prevalent natural biomacromolecules, has drawn increasing attention due to its good film-forming ability, superior biocompatibility, excellent degradability, and commercial availability at a relatively low cost, but has few applications in flexible electronics. Here, we report a method for preparing flexible TCF based on naturally degradable material—fish gelatin, in which silver nanowires and Ti₃C₂T_x flakes were used as conductive fillers. The obtained TCF has low roughness (RMS roughness = 5.62 nm), good photoelectric properties (R_s = 25.2 Ω/sq., T = ca.85% at 550 nm), strong interfacial adhesion and good degradability. Moreover, the film showed excellent application in the field of EMI shielding and green light OLED device. We believe that these TCFs will shine in the smart wearable field in the future.

KEYWORDS

transparent conductive films, fish gelatin, degradable, silver nanowires, Ti₃C₂T_x

1 Introduction

In the era of 5G internet, with the fast growth of flexible electronic technology, electronic gadgets prepared based on transparent conductive films (TCFs) along with organic light-emitting diodes (OLED) (Koo et al., 2010), antennae (Bengio et al., 2019), solar cells (Li et al., 2010), etc., have significantly enhanced and expanded people's daily life. However, the service life of electronic devices is limited, it will invariably be damaged and lose functionalities during usage, resulting in electronic waste (E-waste) (Islam et al.,

2020). The global annual output of E-waste is about 40 metric tons, accounting for 5% of the total global solid wastes (Hazra et al., 2019). E-wastes are difficult to biodegrade and contain large amounts of harmful metals (Cd, Hg, Pb, Cr) and hazardous chemicals, which can penetrate plants and animals through soil and groundwater and have long-term consequences on the entire ecological system. E-waste has risen to the top environmental issue in recent years.

To alleviate the pressure of E-waste on environmental protection, many scholars have proposed to use naturally degradable materials to replace traditional petroleum-derived plastics like poly dimethyl siloxane (PDMS) (Wang D. et al., 2020), polyethylene terephthalate (PET) (Wang T. et al., 2020), polyethylene (Zardetto et al., 2011), polyimide (Bae et al., 2016), polyurethane (Wang, et al., 2019), etc., to prepare “green” flexible wearable electronic devices. Tao et al. (2017) made cellulose nano paper from sugarcane bagasse for field-effect transistors; Yang et al. (2020) novelty use a self-supporting natural dextran membrane as the gate dielectric to achieve an ultra-flexible and degradable organic synaptic transistor; Xia et al. (2020) presented a technique for producing optically transparent wood by changing the wood slignin structure with a solar-assisted chemical brushing technique, and the transparent wood film may be employed as an electronic device substrate. Although the transparent substrates obtained by the aforesaid methods can be utilized to prepare green electronic devices, the costs were high, the processes were complicated, and the transparency of the prepared films was poor. Therefore, a simple method to prepare low-cost and high-performance transparent substrates has emerged as a critical link to solve the problem.

Gelatin (Etxabide et al., 2016), one of the most prevalent natural biomacromolecules, has been widely used in recent years because of its attributes such as good film-forming ability, superior biocompatibility, excellent degradability, and commercial availability at a relatively low cost. The traditional raw materials of gelatin production are the skins and bones of pigs and cattle. However, due to the religious culture and the risk of disease transmission, fish gelatin (FG) has gradually become an alternative to mammalian gelatin (Hosseini et al., 2013). FG could be obtained from fish scales, which are inedible wastes that account for about 3% of the annual production of the 70.5 million metric tons of fish, making it highly cost-efficient and sustainable; these advantages make FG a perfect candidate for transparent substrates (Zhang J. et al., 2020). However, FG-based films have relatively weak mechanical properties which can be improved by blending with other biodegradable polymers which have gradually become an innovative approach to improve the cost-performance ratio of the resulting films. Poly (vinyl alcohol) (PVA) has favorable biodegradability, good mechanical properties, and excellent film-forming ability, which can be mixed with FG to

improve the physical properties of the substrates due to the formation of hydrogen bond between themselves (Ghaderia et al., 2019).

Currently, indium tin oxide (ITO) (Kang et al., 2020) has become a popular conductive material for electronic applications, whereas it has a lot of limitations, including the scarcity of indium, the high-temperature deposition process, and the fragile nature, all of which limit its widespread application in next-generation flexible electronic devices. A significant amount of work has been expended in the search for optimal replacement conductive materials, such as carbon nanotubes (CNTs), graphene, metal nanowires, conductive polymers, etc. (Jing et al., 2020; Zhao et al., 2020; Zhu et al., 2020). Among these candidates, silver nanowires (AgNWs) have piqued the interest of researchers because to their outstanding intrinsic electrical conductivity, superb optical transparency, high flexibility, and low processing temperature. However, owing of the substantial contact resistance between nanowires, pure AgNWs TCFs often display low conductivity, inadequate electrical stability, and poor mechanical flexibility, severely limiting their applicability (Chen et al., 2020).

Since the first discovery of the two-dimensional (2D) nanomaterial $Ti_3C_2T_x$ in 2011 (Liu et al., 2019), MXenes (transition metal carbides, carbonitrides, and nitrides) have been widely used in energy storage devices, water desalination, and electromagnetic radiation protection due to its superior electrical conductivity, hydrophilic surfaces, and large specific surface area. Nevertheless, the sheet-like structure of MXenes makes it easy to restack and aggregate, which may reduce accessible surfaces and slow transports of electrons and ions (Liu et al., 2018).

For the preparation of high-performance TCFs and applications in flexible wearable optoelectronic devices, it is necessary to combine the 1D AgNWs and 2D MXene nanosheets to build a new high-efficiency 3D conductive network. To overcome the drawbacks that the TCFs prepared by the traditional solution coating method are easy to peel off from the substrate, we integrated the 3D conductive network onto the FG/PVA substrate by a simple solution method to obtain a new type of “green” TCFs. Interestingly, the TCFs still exhibited good conductivity and transparency, and the interfacial adhesion of the film could be improved, which were of great significance for the long-term and stable use of electronic devices based on the films.

Here, we successfully fabricated the new type “green” degradable AgNWs/ $Ti_3C_2T_x$ -FG/PVA TCFs by a simple method. The films consist of a high conductivity conductive network composed of AgNWs and $Ti_3C_2T_x$ flakes. The degradable FG/PVA film with low cost, high light transmittance, and good mechanical strength replaces the traditional petroleum derivative materials as the substrate. The excellent performance of the film shows its potential application value as EMI shielding film and optoelectronic device. Besides,

the strategy to develop “green” electronics based on the TCFs may pave a way for the coming of sustainable development and intelligent era in the future.

2 Experimental

2.1 Materials

Ti₃AlC₂ powder (MAX, 400 mesh) was purchased from Jilin Province 11 Technology Co., Ltd. Concentrated hydrochloric acid (HCl, 36.5%), lithium fluoride (LiF, AR, 99%), sodium hydroxide (NaOH, AR, 95%), silver nitrate (AgNO₃, AR, 99%), poly(vinyl pyrrolidone) (PVP; MW = 13,00,000), polyvinyl alcohol (PVA) (Mw of 1,700, 87%–89% hydrolyzed), and aluminum (Al, AR, 99%) were purchased from Shanghai Mackin Biochemical Co., Ltd. N,N'-bis (naphthalene-1-yl)-N,N'-bis (phenyl) benzidine (NPB) and Hydroxyquinoline aluminum (Alq3) (PLT401011G) were purchased from Xi'an Baolite Optoelectronics Technology Co., Ltd. Fish scales were collected from the supermarket. The polyethylene terephthalate (PET; thickness = 0.15 mm) substrate was procured from Carbon Star Technology (Tianjin) Co., Ltd. Deionized (DI) water was used for all experiments.

2.2 Preparation of high-quality few-layer Ti₃C₂T_x by the minimally intensive layer delamination method

The Ti₃C₂T_x flakes were obtained by the minimally intensive layer delamination (MILD) method (Alhabebe et al., 2017). First, 40 ml of 9 M HCl solution and 3.2 g of LiF powders were added into a tetrafluoroethylene beaker and stirred evenly, then 2 g of Ti₃AlC₂ powders were gradually added to the etchant solution under slow stirring at 40°C for 24 h. After the reaction, DI water was added to the beaker, and the resulting solution was repeatedly washed at 3,500 rpm for 5 min until a stable dark green supernatant with a pH of 6 was obtained. Subsequently, the obtained multi-layer Ti₃C₂T_x solution was shaken by hand (200 times) and centrifuged at 3,500 rpm for 5 min. In this process, the solution after each centrifugation did not need to be poured out and continued to be manually shaken. After about 10 cycles, the exfoliation process ended; the above solution was then centrifuged at 3,500 rpm for 30 min to collect the solution. The obtained solution after centrifugation was a few-layer of Ti₃C₂T_x, and the precipitate was unreacted Ti₃AlC₂ and Ti₃C₂T_x with multilayer or incomplete peeling.

To remove the excess LiF impurities in the solution, an appropriate amount of 1 M HCl solution was added into the collected solution, stirred at room temperature for 10 min, and then centrifuged at 3,500 rpm for 5 min until the pH of the solution was 6 to obtain high-quality Ti₃C₂T_x solution (The

concentration of Ti₃C₂T_x solution prepared in this article was ~2 mg/ml).

2.3 Synthesis of AgNWs

The AgNWs were prepared by the polyol method as reported in our previous work (Zhu et al., 2020). The concentration of AgNWs solution prepared in this article was ~3 mg/ml. The fabricated AgNWs and AgNWs film were shown in Supplementary Figure S1.

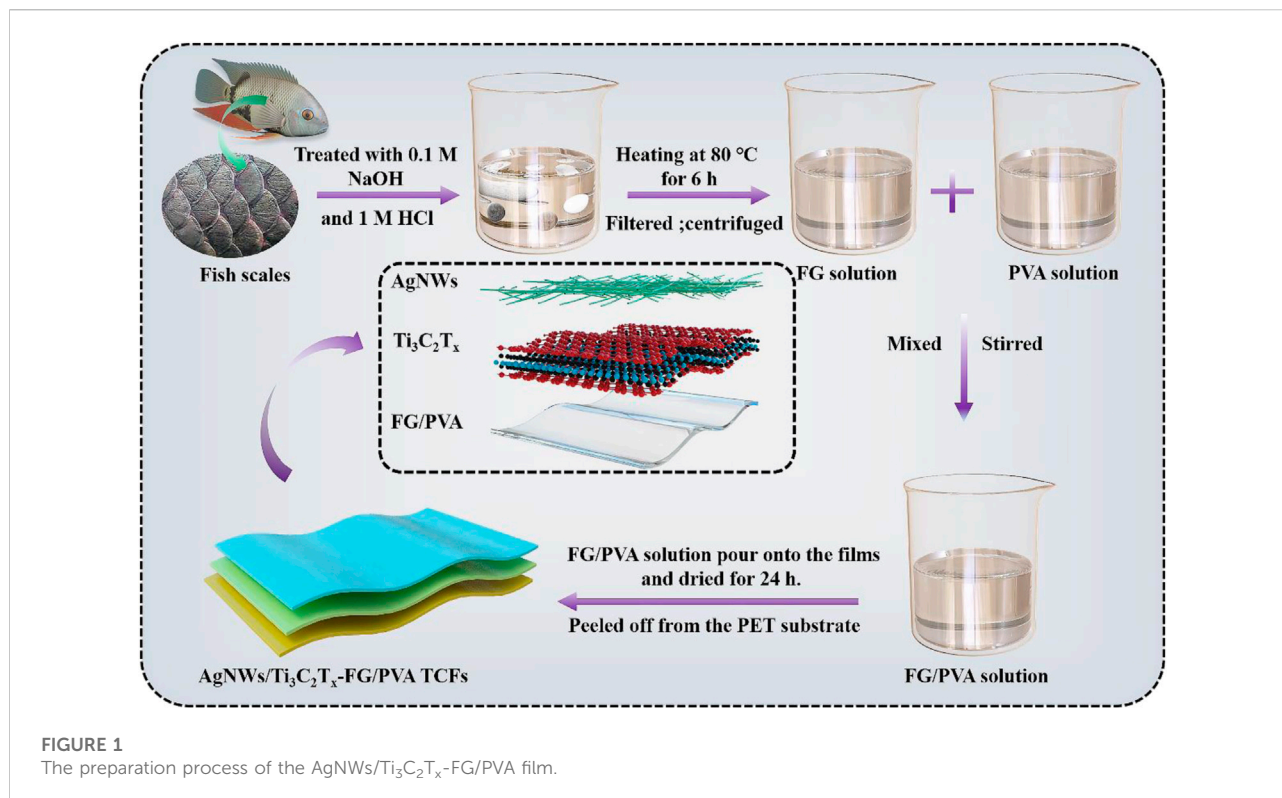
2.4 Fabrication of FG/PVA films

The FG solution was fabricated by a simple method. Firstly, the fish scales collected from the market were washed with water to remove the impurities and dried in the sun and then washed with 0.1 M NaOH and 1 M HCl to remove the minerals. After that, the fish scales and water were added to a sealed beaker at a mass ratio of 1:6 kept at 80°C for 6 h. Then the FG solution was filtered through gauze and centrifuged at 5,000 rpm for 20 min to remove the residue in the solution. Finally, the FG solution with a solids content of about 5 wt.% was obtained. Besides, PVA solution (5 wt.%) was prepared by dissolving PVA in distilled water at 90°C under vigorous stirring for 4 h. The different ratio FG and PVA solutions (1:0, 1:0.5, 1:1, 1.5, 1:2) were mixed and stirred at 80° for 30 min, and glycerin was added to the mixture as a plasticizer. Finally, the FG/PVA solutions were poured and dried in the mold at room temperature for 24 h to obtain the FG/PVA films.

2.5 Preparation of the AgNWs/Ti₃C₂T_x-FG/PVA films

The preparation process of the AgNWs/Ti₃C₂T_x-FG/PVA film was shown in Figure 1. The PET substrates were cut into 4 × 4 cm² size, to remove the contaminants on PET surfaces, it was immersed in acetone and ultrasonic for 30 min, then dried and set aside. Besides, the pristine Ti₃C₂T_x solution and AgNWs solution were diluted to 1 and 1.5 mg/ml, respectively to ensure the smooth spraying process.

The AgNWs/Ti₃C₂T_x-PET films were prepared as followed: At first, PET substrates were fixed on the heating plate (the heating temperature was set to 60°C). Next, the Ti₃C₂T_x solution and AgNWs solution with the volume ratio of 0.5:1 were gradually sprayed onto the PET substrates through the airbrush (Fuso Seiki Co. Ltd., Japan) under certain spray conditions (the outlet pressure of the airbrush was 0.5 MPa, and the distance between the airbrush nozzle and the heating table was 25 cm) to avoid the coffee-ring effect. A series of AgNWs/Ti₃C₂T_x-PET TCFs with different sheet resistance



were fabricated by varying the spray-coating volume. In the end, the AgNWs/Ti₃C₂T_x-PET films were dried in a vacuum oven for later processing.

For AgNWs/Ti₃C₂T_x-FG/PVA films, the AgNWs/Ti₃C₂T_x-PET films were fixed in the stainless-steel molds; and then the same amount of FG/PVA solution with different ratios were poured onto the films and dried at room temperature for 24 h. After drying, the AgNWs/Ti₃C₂T_x-FG/PVA films were peeled off from the PET substrate and stored in a vacuum glove box for later use.

2.6 Measurement of EMI shielding performance

The EMI shielding test was using an AgilentN5244A vector network analyzer in 8–12 GHz (X-Band) with sample sizes of 22.58 × 10.14 mm² based on the waveguide method.

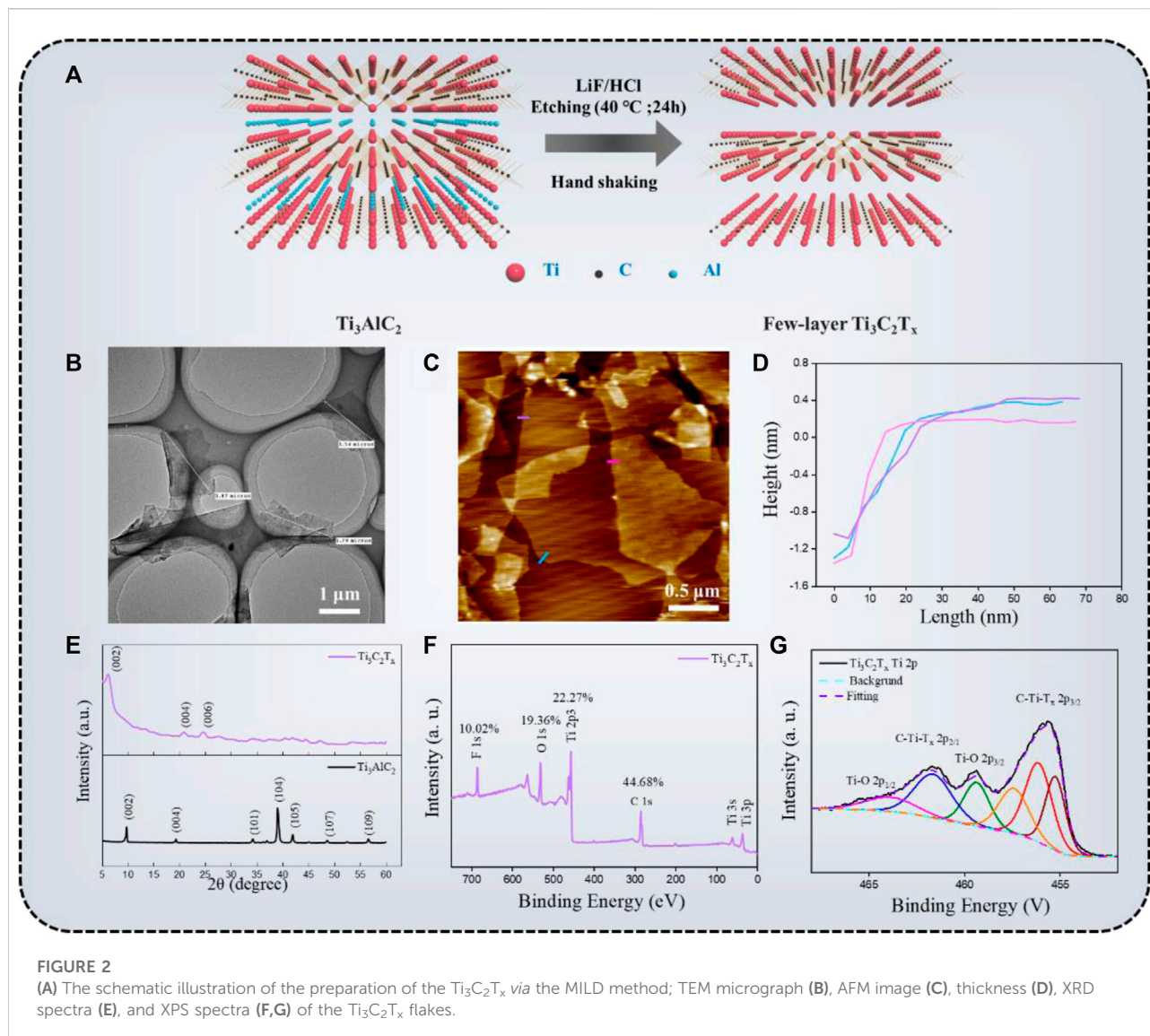
2.7 Fabrication of OLEDs using AgNWs/Ti₃C₂T_x-FG/PVA TCFs as anode

The OLEDs which using AgNWs/Ti₃C₂T_x-FG/PVA TCFs as anode was prepared as reported in our previous work (Wang D. et al., 2020). The OLED structures in this study were AgNWs/

Ti₃C₂T_x-FG/PVA/PEDOT: PSS (20 nm)/NPB (40 nm)/Alq3 (60 nm)/LiF (1 nm)/Al (80 nm). All of the organic materials were thermally evaporated onto the patterned anodes using a thermal evaporation coating system at a pressure of approximately 7 × 10⁻⁴ Pa.

2.8 Characterization

The obtained samples were characterized by the transmission electron microscopy (TEM, Hitachi H-800), X-ray diffraction (XRD, D8 Discover, Bruker, Germany), X-ray photoelectron spectroscopy (XPS, Thermo Fisher, United States), UV-Vis spectrophotometer, Field-emission scanning electron microscopy (FE-SEM) (Hitachi S-4800), Fourier-transform infrared spectroscopy (FT-IR, TENSOR 37, Germany), Testing machine (TVT-300Xp, TexVol Instruments, Viken, Sweden), the sheet resistance device (Keithley 2,700 multi-meter), ultraviolet photoelectron spectroscopy (UPS, Thetaprobe Thermo). Adhesive tape (Scotch Magic Tape, 3M, United States) was utilized to evaluate the adhesion of the films. The performance of the OLEDs was characterized by an optical detection system for OLED display panels developed by Suzhou Fstar Scientific Instrument Co., Ltd. Electromagnetic parameters of composite films were obtained using a network analyzer

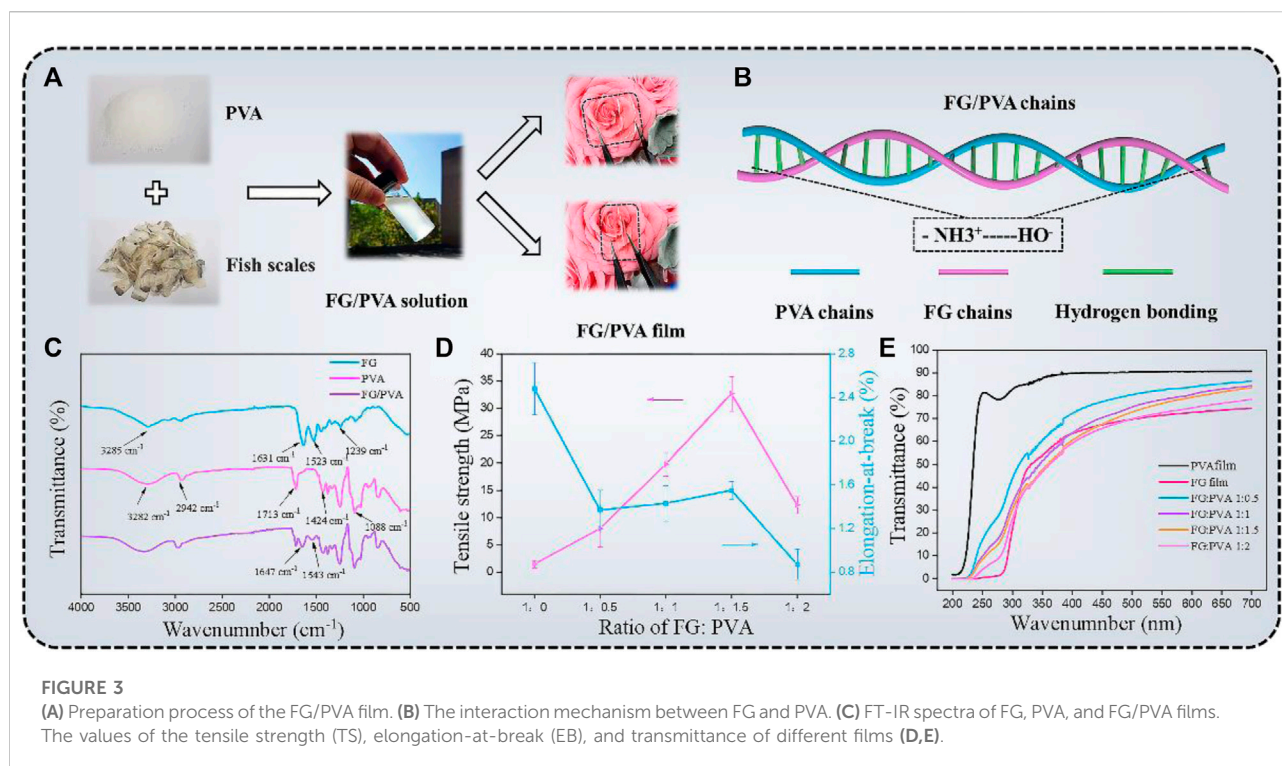


(Agilent Technologies N5244A) in the frequency ranges of 8.2–12.4 GHz (X-band) at room temperature.

3 Results and discussion

The schematic illustration of the preparation of the $\text{Ti}_3\text{C}_2\text{T}_x$ via the MILD method and property characterizations are shown in Figure 2. In Figure 2A, the $\text{Ti}_3\text{C}_2\text{T}_x$ flakes were obtained by the MILD method. The MAX phase- Ti_3AlC_2 powder was etched in the HCl/LiF solutions at 40°C for 24 h. The Al layers were successfully etched by the *in-situ* formed HF. Besides, the multi-layered- $\text{Ti}_3\text{C}_2\text{T}_x$ sheets were further exfoliated to a few-layer- $\text{Ti}_3\text{C}_2\text{T}_x$ by manual hand-shaking (no sonication). From the TEM image (Figure 2B) we can see, the average lateral size of $\text{Ti}_3\text{C}_2\text{T}_x$ nanosheets was $1.7 \pm 0.2 \mu\text{m}$, and these

flakes have clear and neat edges without visual holes, indicating that the MILD method can overcome the shortcomings of excessive flake defects caused by the sonication (Weng et al., 2018). AFM test (Figures 2C,D) was another method to characterize the quality of $\text{Ti}_3\text{C}_2\text{T}_x$. According to Ahn's report (Ahn et al., 2020), the thickness of the single $\text{Ti}_3\text{C}_2\text{T}_x$ flake was about 1 nm, but the average thickness of $\text{Ti}_3\text{C}_2\text{T}_x$ sheets we obtained was ~ 1.5 nm. This was attributed to our AFM measurement's high sensitivity, which identifies surface functional groups and/or adsorbed molecules on and under the flake. The crystal structure of Ti_3AlC_2 and $\text{Ti}_3\text{C}_2\text{T}_x$ particles were further confirmed by XRD patterns (Figure 2E). Compared with Ti_3AlC_2 , many diffraction peaks of $\text{Ti}_3\text{C}_2\text{T}_x$ disappeared after the Al layers were etched. Moreover, the (002) peak shifted from 9.7° to 6.2° , and the corresponding c-lattice spacing of the $\text{Ti}_3\text{C}_2\text{T}_x$ was 25.1 \AA , which is in



agreement with literature data (Zhou et al., 2019). The chemical composition of the $\text{Ti}_3\text{C}_2\text{T}_x$ nanosheets was examined by XPS spectra. The Ti, C, F, and O were discovered in the survey spectra, while the F and O elements were acquired from the etching agent. The XPS spectrum of Ti_{2p} was shown in Figure 2G, the peaks at 455.7 eV ($\text{sp}_{3/2}$) and 461.6 eV ($\text{sp}_{1/2}$) represent a contribution from Ti-C bonds, and the peaks at 459.3 and 463.6 eV correspond to Ti-O bonds (Ahn et al., 2020). The weak intensity of the Ti-O bonds means the prepared $\text{Ti}_3\text{C}_2\text{T}_x$ flakes have no sign of oxidation. According to the above evidence, it showed that the few-layer, uniform diameter distribution, and unoxidized $\text{Ti}_3\text{C}_2\text{T}_x$ flakes were successfully prepared.

The FG/PVA films were synthesized by the solution casting method. As shown in Figure 3A, FG was extracted from natural fish scales and then mixed with PVA (glycerin was added as a plasticizer to improve the processing property of the film), then the mixture solution was poured into the mold and dried at room temperature to obtain FG/PVA film. Figure 3B was the schematic of the interaction mechanism between the FG and PVA chains. With the addition of PVA to FG, the two chains could entangle with each other and form hydrogen bonds, resulting in a hybrid film with better performance. The interactions between PVA and FG were analyzed by FT-IR measurement (Figure 3C). The four typical peaks in the FT-IR spectra of FG film were located around 3,285, 1,631, 1,523, and 1,239 cm^{-1} , which were related to amide A (N-H stretching), amide-I (C=O stretching and the stretching

vibration of O-H groups), amide-II (N-H bending), and amide-III (C-N stretching and N-H bending or vibrations of CH_2 groups in glycine), respectively (Etxabide et al., 2016). In the spectrum of PVA film, the strong and broad absorption peak at about 3,282 cm^{-1} was attributed to the stretching vibration of hydroxyl groups (O-H). Besides, the absorption peaks at 2,942, 1,713, 1,424, and 1,088 cm^{-1} were corresponding to C-H stretching, C=O stretching, O-H bending, and C-O stretching, respectively (Zhang X. et al., 2020). As for the FT-IR spectrum of FG/PVA film, the characteristic peaks of FG and PVA appeared simultaneously in the spectrum of the hybrid film, which indicated that the FG was compatible with PVA. In addition, the position of the amide-II peak in the FG/PVA film shifted from 1,523 cm^{-1} to 1,543 cm^{-1} and the amide-I peak shifted from 1,631 cm^{-1} to 1,647 cm^{-1} . The formation of various types of intra/intermolecular hydrogen bonds between N-H and O-H groups was considered to be the mechanism for this (Ghaderia et al., 2019).

The mechanical strength and flexibility were important index to evaluate the film performance. The values of the tensile strength (TS), elongation-at-break (EB) of different films were exhibited in Figure 3D. FG film (FG:PVA = 1:0) has low TS (1.5 MPa \pm 0.72 MPa) but high EB (248% \pm 24%). To enhance the mechanical strength of the film, PVA was introduced into FG to fabricate the FG/PVA film. The development of intermolecular hydrogen bonding between FG and PVA increased the TS of the hybrid film to 32.67 MPa \pm 3.16 MPa

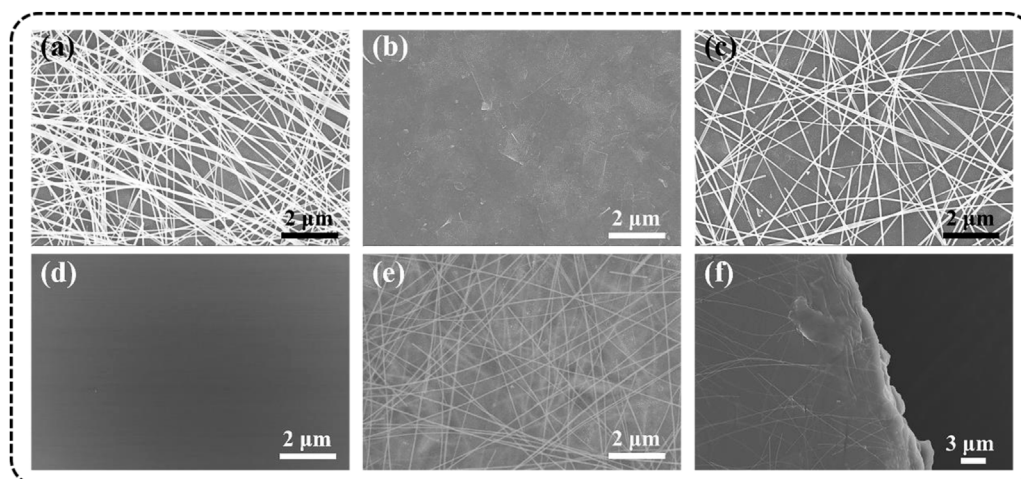


FIGURE 4

SEM images of different films: (A) AgNWs-PET, (B) $\text{Ti}_3\text{C}_2\text{T}_x$ -PET, (C) AgNWs/ $\text{Ti}_3\text{C}_2\text{T}_x$ -PET, (D) FG/PVA, (E) surface, and (F) profile of AgNWs/ $\text{Ti}_3\text{C}_2\text{T}_x$ -FG/PVA.

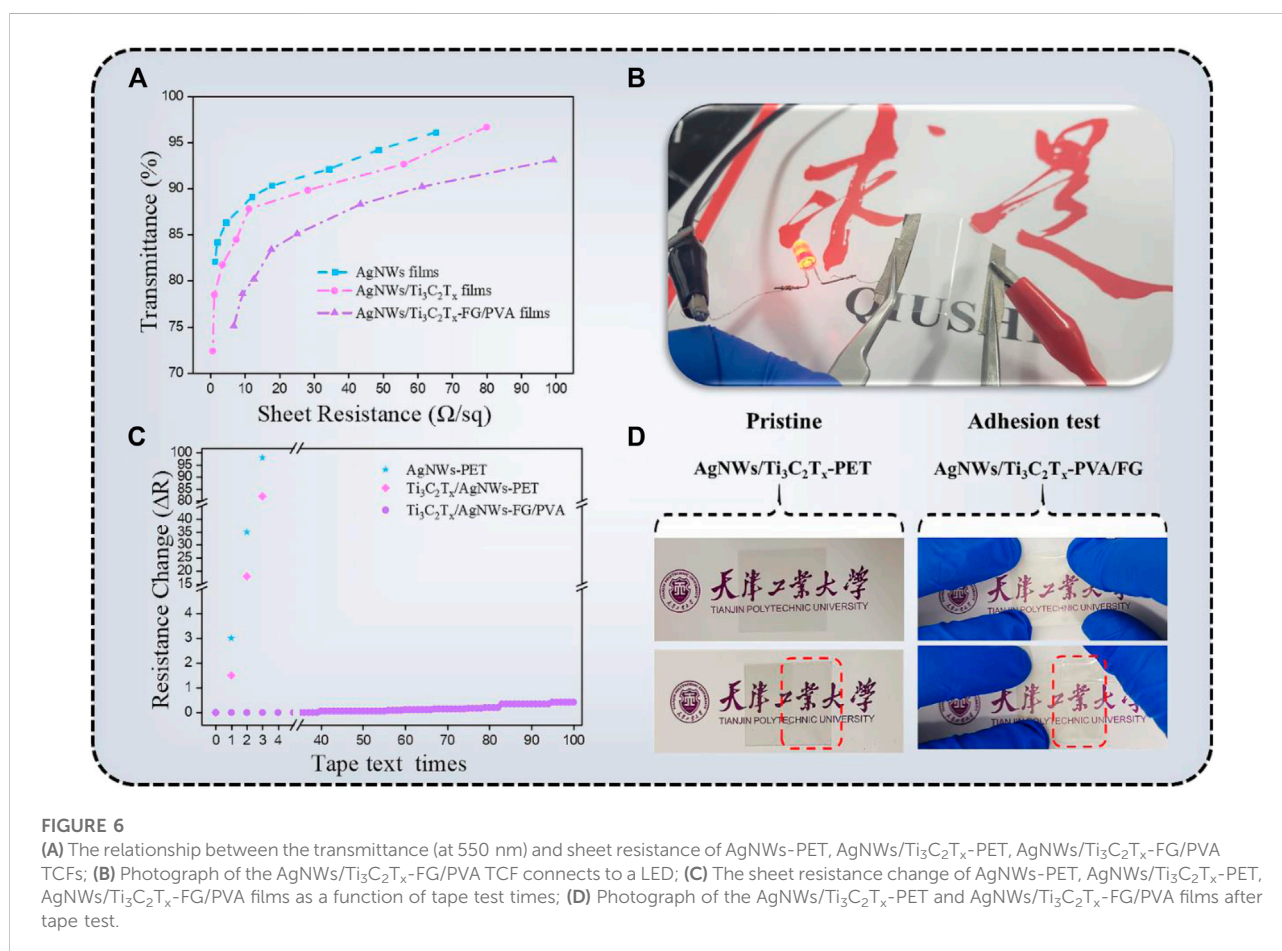
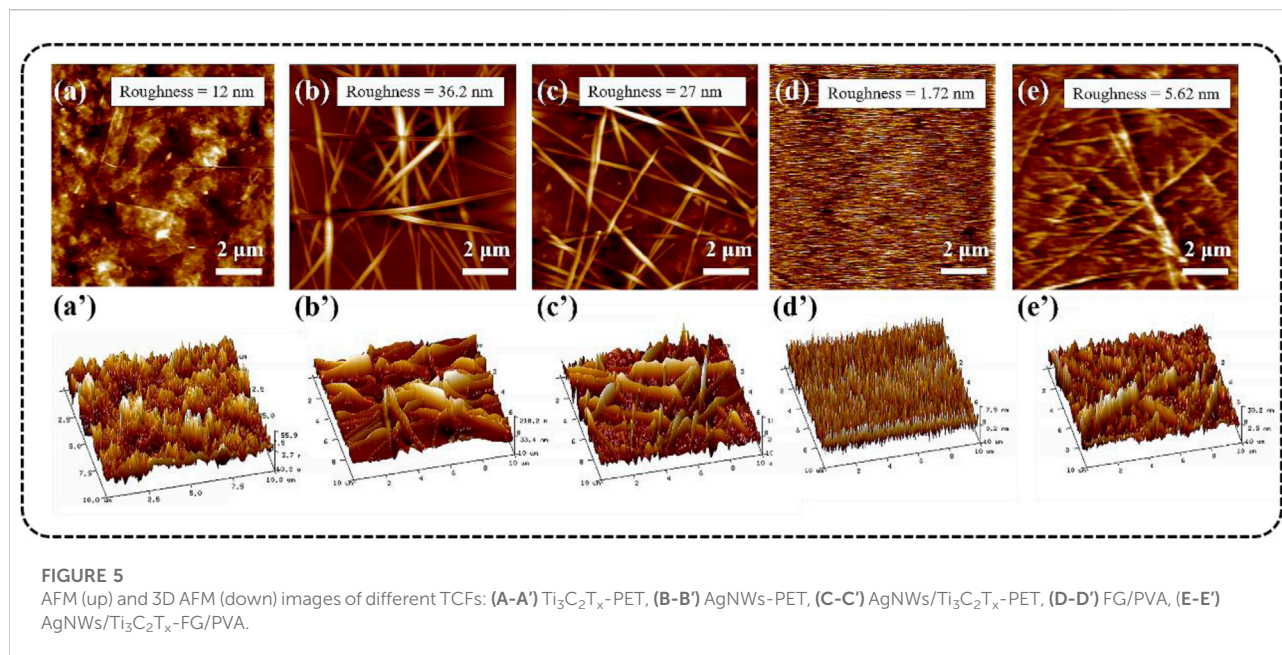
(FG:PVA = 1:1.5) with the addition of PVA. Excess PVA molecules were present in free form in the hybrid film as the fraction of PVA continued to rise, resulting in a reduction in tensile strength (Uranga et al., 2016).

A highly transparent substrate was also a crucial prerequisite for the preparation of high-performance optoelectronic devices. The transmittance of the hybrid film with different PVA addition amounts was investigated by UV-vis spectrometer (Figure 3E). The optical transmittance at 550 nm of different films (FG; FG/PVA 1:0.5; FG/PVA 1:1; FG/PVA 1:1.5; FG/PVA 1:2; PVA) were found to be 82.47%, 78.19%, 76.52%, and 72.47%, respectively. Considering the mechanical properties and transmittance of the film, the optimal ratio of FG: PVA was 1:1.5. The FG: PVA film, in particular, remained undamaged after being submerged in several organic solvents for 24 h, demonstrating high chemical stability (Supplementary Figure S2) (Zhang X. et al., 2020).

The surface morphology of different TCFs was characterized by SEM. All the TCFs (AgNWs-PET, $\text{Ti}_3\text{C}_2\text{T}_x$ -PET, and AgNWs/ $\text{Ti}_3\text{C}_2\text{T}_x$ -PET) were prepared by the spray-coating method, which makes the conductive inks evenly coated on the substrate; moreover, they all exhibited clean surfaces without impurities. As for AgNWs-PET film (Figure 4A), the AgNWs stacked loosely and connected simply, and the junctions exhibited distinct outlines (Liang et al., 2017). When the AgNWs were deposited on the $\text{Ti}_3\text{C}_2\text{T}_x$ layer (Figure 4B), the “voids” in the AgNWs conductive network would be filled (Figure 4C) and the elemental maps of Ag, Ti, and C on the surface prove the uniform distribution of $\text{Ti}_3\text{C}_2\text{T}_x$ and AgNWs (Supplementary Figure S3). In addition, 1D AgNWs and 2D $\text{Ti}_3\text{C}_2\text{T}_x$ flakes could form a dense 3D conductive network, which not only provides more carrier transmission paths to reduce the resistance of the

film but also reduces the roughness of the film. From the SEM image of FG/PVA film, we can know that the hybrid film had smooth and flat surfaces, was free of pores, and had good structural integrity (Figure 4D), which proved the good compatibility between FG and PVA and consistent with the previous report (Ghaderia et al., 2019). Through a simple solution casting method, we successfully integrated the 3D conductive network onto the surface of the substrate and obtained the novel TCFs. In the SEM images of AgNWs/ $\text{Ti}_3\text{C}_2\text{T}_x$ -FG/PVA film (Figures 4E,F), the AgNWs/ $\text{Ti}_3\text{C}_2\text{T}_x$ layer was partially encased in the cured FG/PVA film and the conductive layer kept intact. The changes of the roughness, conductivity and mechanical properties of the AgNWs/ $\text{Ti}_3\text{C}_2\text{T}_x$ -FG/PVA film compared with the AgNWs/ $\text{Ti}_3\text{C}_2\text{T}_x$ -PET film will be discussed as followed.

The tapping mode AFM (2D) images of different TCFs were shown in Figures 5A–E, and the 3D AFM images (Figures 5A–E) corresponding to the height patterns further visually confirmed the surface features of the films. The root means square (RMS) roughness of the $\text{Ti}_3\text{C}_2\text{T}_x$ -PET and AgNWs-PET film was 12.0 and 36.2 nm, respectively. From their images, it can be seen that the $\text{Ti}_3\text{C}_2\text{T}_x$ flakes and AgNWs were evenly distributed on the PET substrate and overlap each other, which was consistent with the SEM results. As the $\text{Ti}_3\text{C}_2\text{T}_x$ nanosheet may cover the “holes” in the AgNWs networks, the roughness of the film (AgNWs/ $\text{Ti}_3\text{C}_2\text{T}_x$ -PET) reduced to 27.0 nm. For optoelectronic devices using TCFs as an anode, the main problem was the TCFs’ high surface roughness, which might allow these materials to penetrate through the active layer to the counter electrode, resulting in short circuits in the devices. To solve this problem, we transferred the conductive layer onto the



flat FG/PVA film (RMS roughness = 1.72 nm) surface. This method can effectively minimize the roughness of the film while maintaining the integrity of the coating. The RMS roughness of the AgNWs/Ti₃C₂T_x-FG/PVA film was only 5.62 nm, which has a broad application prospect in the field of flexible wearable devices.

Among several performance indicators of TCFs, photoelectric properties are the most critical physical factors in photovoltaic devices. The transmittance (*T*) at 550 nm (PET substrate was used as a blank contrast sample) as a function of sheet resistance (*R_s*) of different TCFs was plotted in **Figure 6A**. All the films were obtained by evenly spraying the conductive inks onto the substrates, which can ensure the formation of the conductive networks, and free from notorious percolation problems. The AgNWs-PET film shows excellent photoelectric properties (*T* < 90%; *R_s* < 20 Ω/sq) because AgNWs have high electronic density, excellent conductivity, and high transmittance in visible light. According to Dillon's report (Dillon et al., 2016), MXenes have metallic conductivity (the electrical conductivity of Ti₃C₂T_x sheets was calculated to be 4,762.5 S/cm in this paper), which is a result of metal-like high free-electron density and a sheet-like structure of individual nanosheets. The characteristic resistance of the Ti₃C₂T_x-PET film was 432.6 Ω/sq. with an optical transmittance of 75.2% at 550 nm as shown in **Supplementary Figure S4**.

According to the SEM and AFM analysis, it can be seen that for this 3D conductive network (AgNWs/Ti₃C₂T_x), on the one hand, the Ti₃C₂T_x flakes filling the holes in AgNWs' network can minimize the roughness of the film; on the other hand, this nanosheet with remarkable conductivity can create several carriers transport channels, lowering the film's surface resistance (AgNWs/Ti₃C₂T_x-PET; *R_s* = 8.5 Ω/sq., *T* = ca. 85% at 550 nm). Compared with AgNWs/Ti₃C₂T_x-PET film, the resistance of AgNWs/Ti₃C₂T_x-FG/PVA film has a certain increase, and its characteristic resistance was *R_s* = 25.2 Ω/sq., *T* = ca. 85.1% at 550 nm. The reason for the increase of resistance can be attributed to the fact that part of the AgNWs/Ti₃C₂T_x conductive layer embedded in the FG/PVA film, which may lead to the interruption of some conductive paths. **Figure 6B** shows that the AgNWs/Ti₃C₂T_x-FG/PVA film was put into a circuit connected with a LED light, showing its good photoelectric performance and flexibility.

Low sheet resistance and good transmittance were both necessary for viable optoelectronics applications. The performance of AgNWs/Ti₃C₂T_x-FG/PVA film was evaluated using the figure of merit (FoM), which is defined as the ratio of electrical conductivity (*σ_{dc}*) to optical conductivity (*σ_{op}*). The FoM was estimated using the following formula (Zhao et al., 2020):

$$\frac{\sigma_{dc}}{\sigma_{op}} = \left[\frac{188.5 (\Omega)}{R_s} \frac{\sqrt{T}}{(1 - \sqrt{T})} \right] \quad (1)$$

TABLE 1 Optoelectrical properties of the AgNWs/Ti₃C₂T_x-FG/PVA films.

Samples	1	2	3	4	5	6	7	8
<i>T</i> (%)	93.1	90.2	88.3	85.1	83.4	80.2	78.6	75.1
<i>R_s</i> (Ω/sq.)	99.3	61.3	43.5	25.2	17.7	12.7	9.3	6.8
<i>σ_{dc}/σ_{op}</i>	52.2	58.1	67.5	89.1	112.1	127.3	158.4	180.1

where *T* is the TCFs' transmittance (at 550 nm), and *R_s* is their sheet resistance. **Table 1** showed the values of *σ_{dc}/σ_{op}* for the AgNWs/Ti₃C₂T_x-FG/PVA films; all the samples show excellent performance.

For the various devices based on TCFs, good adhesion is essential to ensure a long-term and efficient use of devices. Unfortunately, the coatings frequently fall off due to insufficient interfacial adhesion between the conductive layers and substrates, along with cohesion within the TCFs materials, which is the most urgent problem to be solved. Hence, we tested the interface adhesion of the AgNWs-PET, AgNWs/Ti₃C₂T_x-PET, and AgNWs/Ti₃C₂T_x-FG/PVA films with the 3M tape to characterize the adhesion properties. **Figure 6C** showed the sheet resistance change after tape adhesion trials which was calculated using the equation (Da et al., 2017):

$$\Delta R = (R - R_0)/R_0 \quad (2)$$

where *R₀* is the original sheet resistance value; *R* is the sheet resistance after the test. It is clear to see that the sheet resistance of AgNWs-PET and AgNWs/Ti₃C₂T_x-PET film was greatly changed. Although the AgNWs/Ti₃C₂T_x network has great conductivity and mechanical flexibility, it also has drawbacks including excessive surface roughness and poor substrate adhesion. Compared with AgNWs-PET and AgNWs/Ti₃C₂T_x-PET, the conductive layer of AgNWs/Ti₃C₂T_x-FG/PVA was not simply deposited on the substrate, but partly imbedded into the FG/PVA film. This imbedded structure makes the TCFs have strong adhesion to ensure the integrity of the coating during the testing process, and the film transmittance almost remains unchanged.

The images of AgNWs/Ti₃C₂T_x-PET and AgNWs/Ti₃C₂T_x-FG/PVA films before and after the adhesion test intuitively show the difference of adhesion properties between these two type of film as shown in **Figure 6D**. It is obvious that the coating of the AgNWs/Ti₃C₂T_x-PET film was readily detached from PET substrates after the test, while the AgNWs/Ti₃C₂T_x-FG/PVA film without cracking or delamination. Besides, the mechanical stability of the AgNWs/Ti₃C₂T_x-FG/PVA was estimated by bending test, and the resistance of the film remained stable after 1,000 bending times, indicating good flexibility of the film (**Supplementary Figure S5**).

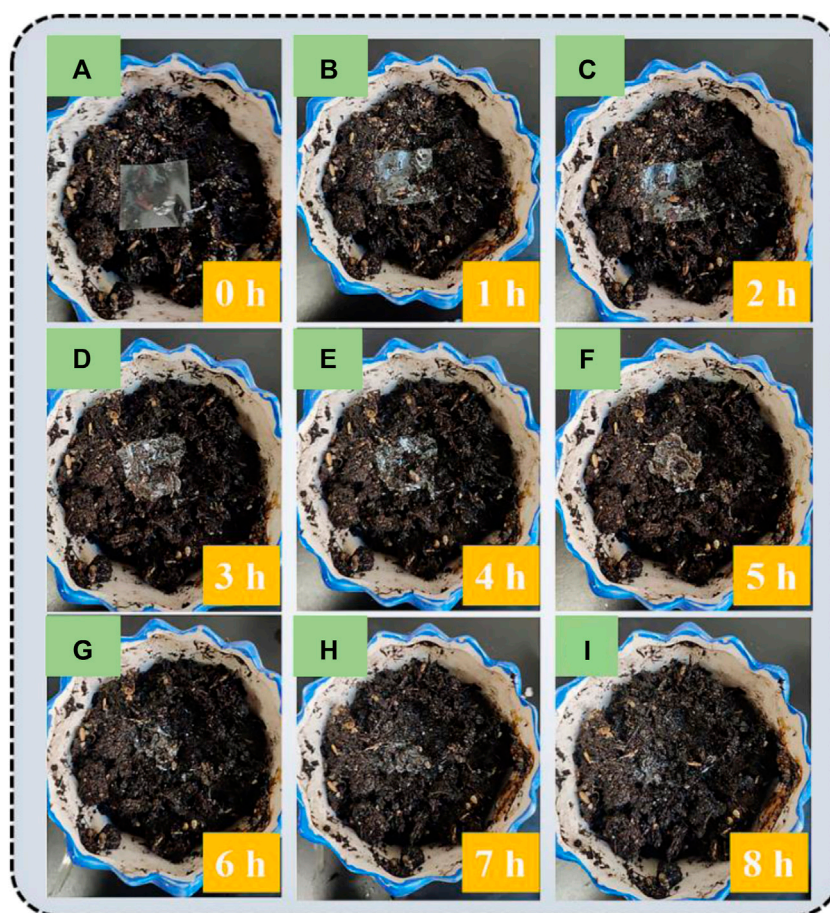


FIGURE 7

The degradable test of AgNWs/Ti₃C₂T_x-FG/PVA film. (A-I) are corresponding to the picture of the film after 0-8h of degradation.

As can be seen from the above description, AgNWs/Ti₃C₂T_x-FG/PVA film has a fairly flat surface, good photoelectric performance, excellent adhesion, and flexibility. However, substituting degradable materials for typical petroleum derivative substrates has been considered as a vital component of degradable “green” devices. Both FG and PVA have admirable biodegradability, which gives degradability to AgNWs/Ti₃C₂T_x-FG/PVA film and devices based on the film; and it will largely alleviate environmental pollution caused by electronic equipment. The degradation test was carried out by burying the film in the soil and observing it every one hour (Verma et al., 2018). We found that the film gradually degraded as shown from Figures 7A–H, and completely degraded after 8 h (Figure 7I), which can achieve “no harm” to the environment.

Because of the high electrical conductivity of AgNWs/Ti₃C₂T_x-FG/PVA films, it can be used as efficiency transparent EMI shielding materials (Iqbal et al., 2020). The EMI shielding performance of different samples (A1, T_{A1} = ca. 90.2%, R_{A1} = 61.3 Ω/sq.; A2, T_{A2} = ca. 85.1%, R_{A2} = 25.2 Ω/sq.;

A3, T_{A3} = ca. 80.2%, R_{A3} = 12.7 Ω/sq.; A4, T_{A4} = ca. 75.1%, R_{A4} = 6.8 Ω/sq.) in X-band (8.2–12.4 GHz) were shown in Figure 8. The measured scattering parameters (S₁₁ and S₂₁) were used to calculate the power coefficients and the EMI SE using the following equations (Zhou et al., 2020):

$$R = |S_{11}|^2, T = |S_{21}|^2 \quad (3)$$

$$1 = A + R + T \quad (4)$$

$$SE_T = -10 \log|T| \quad (5)$$

$$SE_R = -10 \log|1 - R| \quad (6)$$

$$SE_A = -10 \log \left| \frac{T}{1 - R} \right| \quad (7)$$

where *A*, *R*, and *T* are the absorption, reflection, and transmission coefficients, respectively, and *SE_T*, *SE_R*, and *SE_A* are the total microwave shielding, reflection, and absorption effectiveness, respectively. The average EMI SE values of A1, A2, A3, A4 samples were 15.0, 22.4, 26.6, and 33.6 dB, respectively (Figure 8A). It can be seen that the shielding efficiency of the

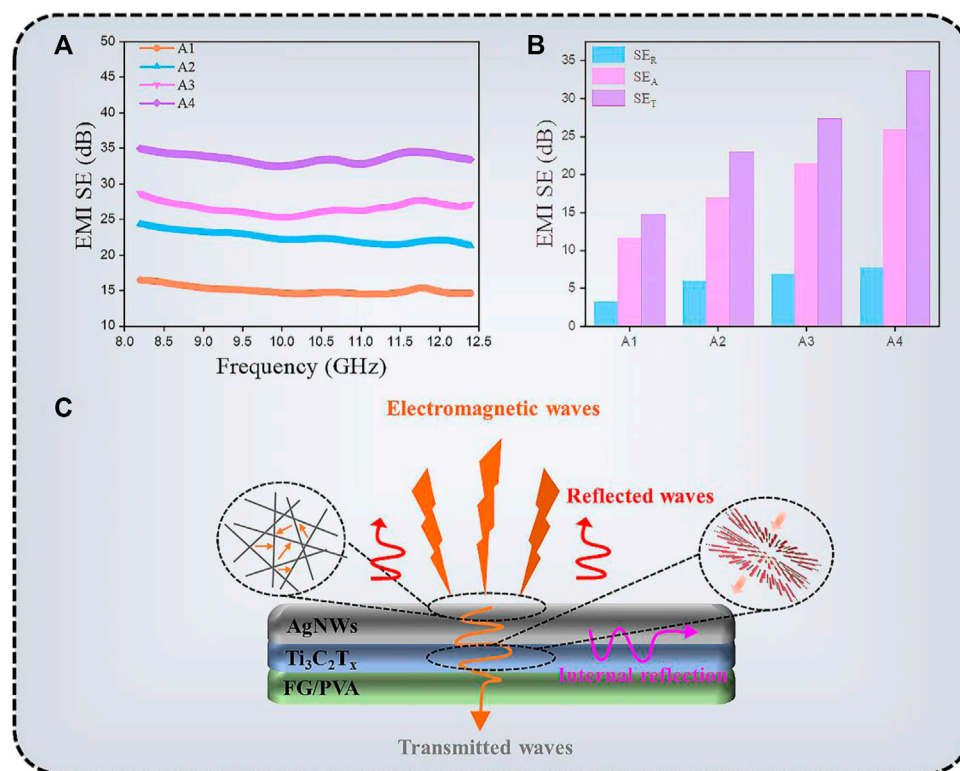


FIGURE 8 (A) EMI shielding performance, (B) EMI SE_T , SE_A , and SE_R values, and (C) the mechanism of EMI shielding of AgNWs/ $Ti_3C_2T_x$ -FG/PVA films.

TCFs increased with the increase of its electrical conductivity. When the transmittance of the TCFs was less than 80%, the shielding performance of the films could meet the requirements of commercial applications (EMI SE value >20 dB). Figure 8B shows the average EMI SE_T , SE_R , and SE_A value, absorption is the primary mechanism of shielding for TCFs. The scheme of EMI shielding mechanism was shown in Figure 8C.

Because of the massive impedance mismatch at the TCF-air interface, most incident EMWs were reflected when they struck the surface of the AgNWs/ $Ti_3C_2T_x$ -FG/PVA film (Zhao et al., 2022). The EMWs interact with the high conductive 3D network, which contribute to ohmic losses, resulting in a drop in energy of the waves. Meanwhile, the good conductive network facilitates the transfer of electrons, making it hard for EMWs to escape from the film until they are dissipated or absorbed in the form of energy. Besides, the large aspect ratio of AgNWs and the sheet structure of $Ti_3C_2T_x$ make the EMWs internal reflection and scattering multiple times in the conductive network, which further promotes the high absorption attenuation of EMWs.

As is known to all, the working mechanism of the OLED device is to apply positive and negative voltages to the anode and cathode of the device, under the action of the hole and electron in an electric field to the corresponding migration in the organic functional layer,

and the light-emitting layer in the composite form excitons, exciton radiative transition that produces light phenomenon. For flexible green light OLED devices based on TCFs, the characteristics of the anode directly affect the performance of the device, including: 1) Good conductivity of the electrode can effectively reduce the device driving voltage; 2) The lower roughness of the electrode can avoid possible short circuits in devices; 3) The higher work function (WF) of the electrode can match the highest occupied molecular orbital (HOMO) energy levels of the hole injection material, which can reduce the potential barrier between the anode and the organic layer, improve the hole injection efficiency, and obtain high-performance devices.

The AgNWs/ $Ti_3C_2T_x$ -PET FG/PVA TCFs can be used as the anode of flexible OLED due to its flat surface, high optical transmittance, excellent electrical conductivity, and proper WF (Kim et al., 2015). The schematic structure and energy diagram of the device are depicted in Figures 9A,B. PEDOT:PSS (WF = 5.2 eV; $\sigma = 1000$ S/m) was used as a hole inject layer on AgNWs/ $Ti_3C_2T_x$ -PET FG/PVA film, which can not only modify the WF, but also further reduce the roughness of the TCFs. Subsequently, NPB (WF = 5.4 eV), Alq3 (WF = 5.7 eV), and LiF/Al were, respectively deposited on the anode by vacuum evaporation as the hole transport layer, luminescent layer, electron transport layer, and cathode. The

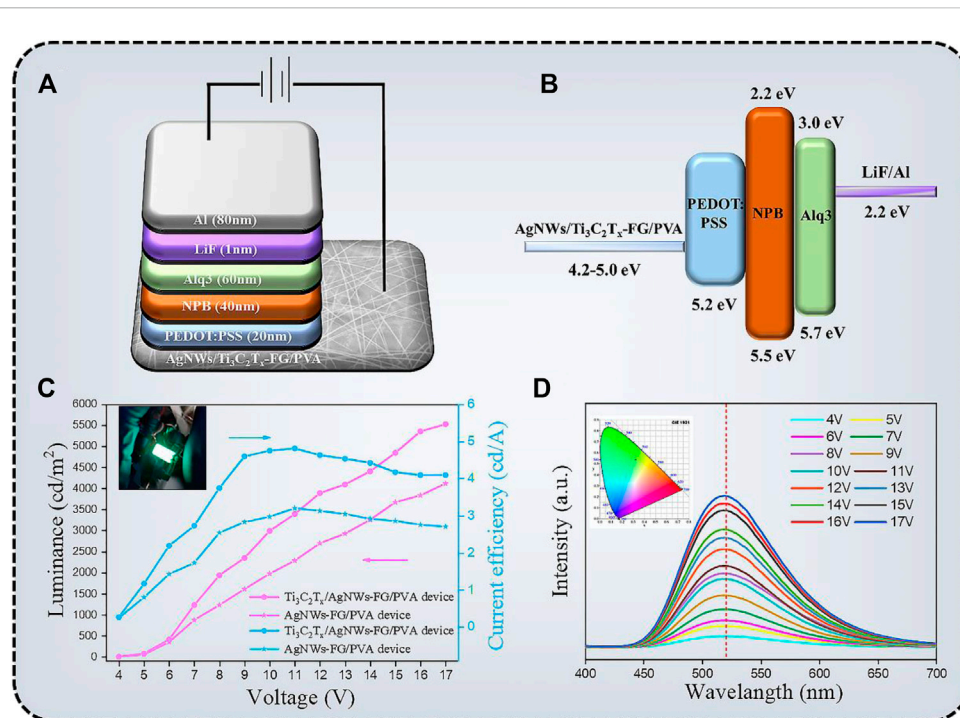


FIGURE 9

(A) The structure of green OLEDs on the AgNWs/Ti₃C₂T_x-FG/PVA anode. (B) The energy diagram of the OLED device. (C) Voltage-Luminance curve and Voltage-Current efficiency curve for the OLED device (inset: the image of OLED device); (D) electroluminescence (EL) spectra of the OLEDs (inset: CIE color coordinates).

relationship between the luminance and current efficiency as a function of voltage for the device are shown in Figure 9C. The maximum luminance of the AgNWs-FG/PVA device was 4,117.3 cd/m² at 17 V, and the maximum current efficiency was 3.21 cd/A at 11 V. In contrast, the AgNWs/Ti₃C₂T_x-FG/PVA device exhibited better performance, which the maximum luminance was 5,525.7 cd/m² at 17 V and the maximum current efficiency was 4.81 cd/A at 10 V. Besides, the external quantum efficiency of the AgNWs/Ti₃C₂T_x-FG/PVA device was shown in Supplementary Figure S6; its maximum external quantum efficiency was 2.55% at 13 V, indicating the good properties of the device. The improved performance of the device was due to the addition of high WF Ti₃C₂T_x flakes (5.0 eV), which could solve the problem of difficulty in injecting holes from the anode into the organic layer caused by low WF of the AgNWs (4.2 eV). Figure 9D shows the electroluminescence (EL) spectra of the AgNWs/Ti₃C₂T_x-FG/PVA device, the electroluminescence peak of the device was at 520 nm, and with the increase of the driving voltage, the peak of the device does not shift, indicating that the device has very excellent chromatographic purity. The spectrometer PR655 was used to measure the color coordinates of green OLEDs. As shown in the inset of Figure 9D, the color coordinates of the device are shown in CIE 1931 color space (0.30, 0.53). Moreover, the high-performance OLED devices using the degradable AgNWs/Ti₃C₂T_x-FG/PVA film

can be degraded in a simple way (as shown in Figure 7) to solve the problem of environmental pollution caused by random disposal of “electronic waste”. This method of preparing degradable OLED devices based on degradable films provides a new idea for the future preparation of environmentally friendly flexible electronic devices.

4 Conclusion

In summary, we demonstrated a method for preparing flexible TCFs based on naturally degradable material-FG, in which AgNWs and Ti₃C₂T_x flakes with excellent electrical conductivity were used as conductive fillers. The film has low roughness, good photoelectric properties, strong interfacial adhesion, and degradability. The good properties of the film are the guarantee of its wide application in various fields. The film showed a certain shielding performance in the field of EMI shielding, in addition, the film can be used as an anode to prepare flexible high-performance OLED device. All the evidence confirmed the potential application value of this new type of TCFs in various fields, and its degradability would alleviate the environmental pollution problems caused by the iteration of electronic products. We believe that these TCFs will shine in the smart wearable field in the future.

Data availability statement

The original contributions presented in the study are included in the article/Supplementary Material, further inquiries can be directed to the corresponding authors.

Author contributions

YW: conceptualization, investigation, methodology, writing–original draft; TW: formal analysis, investigation, methodology, writing–original draft; YL: data curation, methodology; H-ZG: funding acquisition, writing–review and editing; LZ: supervision, writing–review and editing.

Funding

The authors gratefully acknowledge financial support from the Key Scientific Research Projects of Universities of Henan Province (Grant No. 22A430015) and Natural Science Foundation of Tianjin China (Grant No.19JCZDJC37800 and 20YDTPJC01690).

References

- Ahn, S., Han, T. H., Maleski, K., Song, J., Kim, Y., Park, M., et al. (2020). A 2D titanium carbide MXene flexible electrode for high-efficiency light-emitting diodes. *Adv. Mat.* 9, 2000919. doi:10.1002/adma.202000919
- Alhabeib, M., Maleski, K., Anasori, B., Lelyukh, P., Clark, L., Sin, S., et al. (2017). Guidelines for synthesis and processing of two-dimensional titanium carbide ($Ti_3C_2T_x$ MXene). *Chem. Mat.* 29, 7633–7644. doi:10.1021/acs.chemmater.7b02847
- Bae, W. J., Kovalev, M. K., Kalinina, F., Kim, M., and Cho, C. (2016). Towards colorless polyimide/silica hybrids for flexible substrates. *Polymer* 105, 124–132. doi:10.1016/j.polymer.2016.10.023
- Bengio, E. A., Senic, D., Taylor, L., Headrick, R. J., King, M., Chen, P., et al. (2019). Carbon nanotube thin film patch antennas for wireless communications. *Appl. Phys. Lett.* 20, 203102. doi:10.1063/1.5093327
- Chen, W., Liu, L. X., Zhang, H. B., and Yu, Z. Z. (2020). Flexible, transparent, and conductive $Ti_3C_2T_x$ MXene–silver nanowire films with smart acoustic sensitivity for high-performance electromagnetic interference shielding. *ACS Nano* 14, 16643–16653. doi:10.1021/acsnano.0c01635
- Da, S. X., Wang, J., Geng, H.-Z., Jia, S. L., Xu, C. X., Li, L. G., et al. (2017). High adhesion transparent conducting films using graphene oxide hybrid carbon nanotubes. *Appl. Surf. Sci.* 392, 1117–1125. doi:10.1016/j.apsusc.2016.09.143
- Dillon, A. D., Ghidui, M. J., Krick, A. L., Griggs, J., May, S. J., Gogotsi, Y., et al. (2016). Highly conductive optical quality solution-processed films of 2D titanium carbide. *Adv. Funct. Mat.* 26, 4162–4168. doi:10.1002/adfm.201600357
- Etzabadi, A., Leceta, I., Cabezedo, S., Guerrero, P., and de la Caba, K. (2016). Sustainable fish gelatin films: From food processing waste to compost. *ACS Sustain. Chem. Eng.* 4, 4626–4634. doi:10.1021/acssuschemeng.6b00750
- Ghaderia, J., Hosseini, S. F., Keyvanib, N., and Gomez-Guillen, M. C. (2019). Polymer blending effects on the physicochemical and structural features of the chitosan/poly(vinyl alcohol)/fish gelatin ternary biodegradable films. *Food Hydrocoll.* 95, 122–132. doi:10.1016/j.foodhyd.2019.04.021
- Hazra, A., Das, S., Ganguly, A. P., Das, P., Chatterjee, P. K., Murmu, N. C., et al. (2019). Plasma arc technology: A potential solution toward waste to energy conversion and of GHGs mitigation. *Waste Valor. Recycl.* 1, 203–217. doi:10.1007/978-981-13-2784-1_19

Conflict of interest

TW was employed by Sinopec Petroleum Engineering Zhongyuan Corporation.

The remaining authors declare that the research was conducted in the absence of any commercial or financial relationships that could be construed as a potential conflict of interest.

Publisher's note

All claims expressed in this article are solely those of the authors and do not necessarily represent those of their affiliated organizations, or those of the publisher, the editors and the reviewers. Any product that may be evaluated in this article, or claim that may be made by its manufacturer, is not guaranteed or endorsed by the publisher.

Supplementary material

The Supplementary Material for this article can be found online at: <https://www.frontiersin.org/articles/10.3389/fchem.2022.973115/full#supplementary-material>

- Hosseini, S. F., Rezaei, M., Zandi, M., and Ghavi, F. F. (2013). Preparation and functional properties of fish gelatin-chitosan blend edible films. *Food Chem.* 136, 1490–1495. doi:10.1016/j.foodchem.2012.09.081
- Iqbal, A., Sambyal, P., and Koo, C. M. (2020). 2D MXenes for electromagnetic shielding: A review. *Adv. Funct. Mat.* 8, 2000883. doi:10.1002/adfm.202000883
- Islam, A., Rahman, A., Sultana, M., Aziz, A. A., et al. (2020). Advances in sustainable approaches to recover metals from E-waste-A review. *J. Clean. Prod.* 244, 118815. doi:10.1016/j.jclepro.2019.118815
- Jing, L. C., Wang, T., Cao, W. W., Wen, J. G., Zhao, H., Ning, Y. J., et al. (2020). Water-based polyurethane composite anticorrosive barrier coating via enhanced dispersion of functionalized graphene oxide in the presence of acidified multi-walled carbon nanotubes. *Prog. Org. Coat.* 146, 105734. doi:10.1016/j.porgcoat.2020.105734
- Kang, S. K., Kang, D. Y., Park, J. W., Rock Son, K., and Geun Kim, T. (2020). Work function-tunable ZnO/Ag/ZnO film as an effective hole injection electrode prepared via nickel doping for thermally activated delayed fluorescence-based flexible blue organic light-emitting diodes. *Appl. Surf. Sci.* 538, 148202. doi:10.1016/j.apsusc.2020.148202
- Kim, J. H., and Park, J. W. (2015). Foldable transparent substrates with embedded electrodes for flexible electronics. *ACS Appl. Mat. Interfaces* 7, 18574–18580. doi:10.1021/acsami.5b04982
- Koo, W. H., Jeong, S. M., Araoka, F., Ishikawa, K., Nishimura, S., Toyooka, T., et al. (2010). Light extraction from organic light-emitting diodes enhanced by spontaneously formed buckles. *Nat. Photonics* 4, 222–226. doi:10.1038/nphoton.2010.7
- Li, S. S., Tu, K. H., Lin, C. C., Chen, C. W., and Chhowalla, M. (2010). Solution-processable graphene oxide as an efficient hole transport layer in polymer solar cells. *ACS Nano* 4, 3169–3174. doi:10.1021/nn100551j
- Liang, X., Zhao, T., Zhu, P., Hu, Y., Sun, R., and Wong, C. P. (2017). Room-temperature nanowelding of a silver nanowire network triggered by hydrogen chloride vapor for flexible transparent conductive films. *ACS Appl. Mat. Interfaces* 9, 40857–40867. doi:10.1021/acsami.7b13048
- Liu, J., Zhang, H. B., Xie, X., Yang, R., Liu, Z., Liu, Y., et al. (2018). Multifunctional, superelastic, and lightweight MXene/polyimide aerogels. *Small* 14, 1802479. doi:10.1002/smll.201802479

- Liu, L.-X., Chen, W., Zhang, H. B., Wang, Q., Guan, F., and Yu, Z. (2019). Flexible and multifunctional silk textiles with biomimetic leaf-like MXene/silver nanowire nanostructures for electromagnetic interference shielding, humidity monitoring, and self-derived hydrophobicity. *Adv. Funct. Mat.* 29, 1905197. doi:10.1002/adfm.201905197
- Tao, J., Fang, Z., Zhang, Q., Bao, W., Zhu, M., Yao, Y., et al. (2017). Super-clear nanopaper from agro-industrial waste for green electronics. *Adv. Electron. Mat.* 3, 1600539. doi:10.1002/aelm.201600539
- Uranga, J., Leceta, I., Etxabide, A., Guerrero, P., and de la Caba, K. (2016). Cross-linking of fish gelatins to develop sustainable films with enhanced properties. *Eur. Polym. J.* 78, 82–90. doi:10.1016/j.eurpolymj.2016.03.017
- Verma, S., Tripathi, J., Katiyar, M., and Verma, V. (2018). Biodegradable photolithography compatible substrate for transparent transient electronics and flexible energy storage devices. *Appl. Mat. Today* 13, 83–90. doi:10.1016/j.apmt.2018.08.010
- Wang, D., Lin, Y., Hu, D., Jiang, P., and Huang, X. (2020). Multifunctional 3D-MXene/PDMS nanocomposites for electrical, thermal and triboelectric applications. *Compos. Part A Appl. Sci. Manuf.* 130, 105754. doi:10.1016/j.compositesa.2019.105754
- Wang, T., Jing, L. C., Zhu, Q., Sagadevan Ethiraj, A., Fan, X., Liu, H., et al. (2020). Tannic acid modified graphene/CNT three-dimensional conductive network for preparing high-performance transparent flexible heaters. *J. Colloid Interface Sci.* 577, 300–310. doi:10.1016/j.jcis.2020.05.084
- Wang, T., Jing, L. C., Zhu, Q., Sagadevan Ethiraj, A., Tian, Y., Zhao, H., et al. (2019). Fabrication of architectural structured polydopamine-functionalized reduced graphene oxide/carbon nanotube/PEDOT:PSS nanocomposites as flexible transparent electrodes for OLEDs. *Appl. Surf. Sci.* 500, 143997. doi:10.1016/j.apsusc.2019.143997
- Weng, G. M., Li, J., Alhabeb, M., Karpovich, C., Wang, H., Lipton, J., et al. (2018). Layer-by-Layer assembly of cross-functional semi-transparent MXene-carbon nanotubes composite films for next-generation electromagnetic interference shielding. *Adv. Funct. Mat.* 28, 1803360. doi:10.1002/adfm.201803360
- Xia, Q., Chen, C., Li, T., He, S., Gao, J., Wang, X., et al. (2020). Solar-assisted fabrication of large-scale, patternable transparent wood. *Sci. Adv.* 7, 7342. doi:10.1126/sciadv.abd7342
- Yang, Y., Zhao, X., Zhang, C. Y., Tong, Y., Hu, J., Zhang, H., et al. (2020). Ultraflexible, degradable organic synaptic transistors based on natural polysaccharides for neuromorphic applications. *Adv. Funct. Mat.* 30, 2006271. doi:10.1002/adfm.202006271
- Zardetto, V., Brown, T. M., Reale, A., and Di Carlo, A. (2011). Substrates for flexible electronics: A practical investigation on the electrical, film flexibility, optical, temperature, and solvent resistance properties. *J. Polym. Sci. B. Polym. Phys.* 49, 638–648. doi:10.1002/polb.22227
- Zhang, J., Kong, N., Uzun, S., Levitt, A., Seyedin, S., Lynch, P. A., et al. (2020). Scalable manufacturing of free-standing, strong $Ti_3C_2T_x$ MXene films with outstanding conductivity. *Adv. Mat.* 1, 2001093. doi:10.1002/adma.202001093
- Zhang, X., Ye, T., Meng, X., Tian, Z., Pang, L., Han, Y., et al. (2020). Sustainable and transparent fish gelatin films for flexible electroluminescent devices. *ACS Nano* 14, 3876–3884. doi:10.1021/acsnano.9b09880
- Zhao, H., Geng, W., Cao, W. W., Wen, J. G., Wang, T., Tian, Y., et al. (2020). Highly stable and conductive PEDOT:PSS/GO-SWCNT bilayer transparent conductive films. *New J. Chem.* 44, 780–790. doi:10.1039/C9NJ04414K
- Zhao, W., Xu, H., Zhao, J., Zhu, X., Lu, Y., et al. (2022). Flexible, lightweight and multi-level superimposed titanium carbide films for enhanced electromagnetic interference shielding. *Chem. Eng. J.* 437, 135266. doi:10.1016/j.cej.2022.135266
- Zhou, B., Han, X., Li, L., Feng, Y., Fang, T., Zheng, G., et al. (2019). Ultrathin, flexible transparent joule heater with fast response time based on single-walled carbon nanotubes/poly(vinyl alcohol) film. *Compos. Sci. Technol.* 183, 107796. doi:10.1016/j.compscitech.2019.107796
- Zhou, B., Zhang, Z., Li, Y., Han, G., Feng, Y., Wang, B., et al. (2020). Flexible, robust, and multifunctional electromagnetic interference shielding film with alternating cellulose nanofiber and MXene layers. *ACS Appl. Mat. Interfaces* 12, 4895–4905. doi:10.1021/acsmi.9b19768
- Zhu, Z. R., Geng, W., Zhu, Q., Ethiraj, A. S., Wang, T., Jing, L. C., et al. (2020). Highly transparent, low sheet resistance and stable tannic acid modified-SWCNT/AgNW double-layer conductive network for organic light emitting diodes. *Nanotechnology* 32, 015708. doi:10.1088/1361-6528/abb906